

Article

Preliminary Examinations of Phenotypical Changes in Land-Based Long-Term Tumble Culture of *Palmaria palmata*

Stefan Sebök ^{1,*}, Martina Strittmatter ² , Claire M. M. Gachon ³ and Dieter Hanelt ¹

¹ University Hamburg, Department Biology, Institute of Plant Science and Microbiology, Aquatic Ecophysiology and Phycology, 22609 Hamburg, Germany; dieter.hanelt@uni-hamburg.de

² Scottish Association for Marine Science, Oban PA37 1QA, UK; martina.strittmatter@web.de

³ Muséum National d'Histoire Naturelle & Scottish Association for Marine Science, Oban PA37 1QA, UK; claire.gachon@mnhn.fr

* Correspondence: stefan.seboek@uni-hamburg.de

Abstract: Within the last decade, the red alga *P. palmata* gained increasing interest as a food additive in Europe. Traditionally, *P. palmata* is harvested from wild stocks, but higher biomass demands request a shift towards industrial cultivation of this species. Using a land-based tumble culture approach, we have successfully grown *P. palmata* via vegetative propagation over a 2-year period. One year after the initial setup, phenotypic changes represented in the formation of randomly shaped, mostly circular galls and homogeneous greenish–white spots with significantly reduced photosynthetic activity were observed on the algal thalli. With progressing time, galls increased into large flat or sunken structures, whereas the tissue in the center of the greenish–white spots weakened. In later stages, the weakened tissue is disrupted, forming holes in the thallus. In this study, we present observations, microscopy analysis, PAM results, and biotechnological approaches to describe a possible infection of *P. palmata*. Test results showed that light quantity might be the most important factor for the propagation behavior of the infection, whereas the pH level might be secondary, and the nutrient level and biomass density might be of minor relevance. Similarly, changes in light quality could also influence the occurrence of pathological changes in *P. palmata*.



Citation: Sebök, S.; Strittmatter, M.; Gachon, C.M.M.; Hanelt, D. Preliminary Examinations of Phenotypical Changes in Land-Based Long-Term Tumble Culture of *Palmaria palmata*. *Phycology* **2023**, *3*, 503–519. <https://doi.org/10.3390/phyco3040034>

Academic Editor: Peer Schenk

Received: 27 October 2023

Revised: 21 November 2023

Accepted: 27 November 2023

Published: 4 December 2023



Copyright: © 2023 by the authors. Licensee MDPI, Basel, Switzerland. This article is an open access article distributed under the terms and conditions of the Creative Commons Attribution (CC BY) license (<https://creativecommons.org/licenses/by/4.0/>).

Keywords: *Palmaria*; disease; infection; cultivation

1. Introduction

The globally increased demand for seaweed as a raw material in industries as diverse as the food industry, pharmacy, or textile and paper production [1–5] has led to the large-scale mass production of marine macroalgae since the wild seaweed stocks can by no means meet the growing demand in terms of quality and quantity.

However, the quality and quantity of (industrial) seaweed cultivation face challenges. Climate change has led to changes in biotic and abiotic environmental conditions, which in turn promote the spread of pathogens and pests and can mutually influence the biotic components of the habitat [6,7]. Those algal pathogens can have an immense economic impact on algae production. For example, infections by epiphytic marine bacteria led to a 25–30% loss in yielded brown algae *Laminaria japonica* in China [8]. The pathogenic oomycete *Olpidiopsis pyropiae* caused biomass losses of up to 20% in Korean *Porphyra* production [9,10]. In the Philippines and East Africa, the changing environmental conditions resulted, among other things, in the spread of the ice–ice disease, which reduced the annual production yield of the algae *Kappaphycus* sp. and *Euचेuma* sp. by more than 15%, causing revenue losses of over \$ 100 Mill. [11–13].

Possible abiotic stressors known to affect the fitness and resistance of seaweeds to diseases and pests [14] are changes in salinity, light intensity, temperature, or nutritional quality [15]. They can cause epiphytic infestations, which in turn increase the risk of

subsequent infection by opportunistic bacteria or viruses [16,17]. The prevalence of monoculture and the desired uniformity of produced seaweed through clonal or vegetative multiplication, as pursued by the seaweed industry, further increases the vulnerability of the cultivated species to abiotic stressors, pests, and pathogens [18].

Whereas the impact of pathogens and pests on algal cultivation is increasingly evident, knowledge of those organisms is still very scarce. For example, a new oomycete pathogen, *Olpidiopsis palmariae*, has been described in a *Palmaria* hatchery, which affects *Palmaria* spores and, therefore, diminishes the algal recruitment [19]. *P. palmata* is an edible seaweed and is increasingly gaining attention as a health food and cosmetic ingredient as it is a rich source of proteins, vitamins, and antioxidants, which can provide health benefits [20–22]. While *P. palmata* is mostly collected as wild seaweed in Europe, the increased industrial demand calls for different approaches to the alga's reproduction to reduce the dependency on its natural occurrence. In this context, it is crucial to extend the currently limited knowledge of *Palmaria* pathogens.

With the intention to contribute to this discussion, this paper presents the 2-year observation of a land-based culture of the red alga *P. palmata*, which was propagated purely vegetatively and showed increasingly visible signs of a disease (e.g., plaques or green spots). The observations show different stages of pathological deformation of *P. palmata* but also include experimental results regarding photosynthetic changes between healthy and infected thalli as well as laboratory test results on the influence of procedural variations on the symptoms.

2. Materials and Methods

2.1. Algal Material

Studies were conducted using unattached, vegetative growing pieces of the folioid red alga *Palmaria palmata* (L.) Kuntze. Algae were collected on the beach of Grenaa, Denmark (56°25' N, 10°53' E) in May 2020 and cultivated in two 2000 L tumble culture tanks (Meeresalgenland UG, Potsdam, Germany). Before placing thalli in the tumble tanks, algae were treated with 1% sodium hypochlorite solution according to [23] for up to 5 min to eliminate epiphytes.

2.2. Cultivation Medium

Artificial seawater was used as cultivation medium in the culture tanks with a target salinity of 30 practical salinity units (psu) using 30 g of artificial sea salt (Tropic Marin, Dr. Biener GmbH, Wartenberg, Germany) per liter of fresh water. The salinity was checked every second day using a digital refractometer (HI 9033, Hanna Instruments, Vöhringen, Germany). The cultivation medium was not replaced during the whole experimental period of two years to meet the requirements of cost-effective cultivation. However, due to the evaporation of the culture medium, fresh water was added to keep the salinity level stable at 30 psu. Additionally, due to the cleaning processes of the pressure filter, approximately 12 L of fresh artificial seawater were added per month and tank. To avoid the accumulation of algae debris and to ensure low microbiological contamination of the culture medium in each tank, a pressure filter with integrated sponge filter elements and 18-W UV-C-filter (CPF-15000, Varan Motors, Weiswampach, Luxembourg) was used. In combination with a flow pump (Hailea HX8810, Raoping, Guangdong, China), up to 14,000 L of culture medium passed the pressure-sponge-UV-C filter per day and tank.

2.3. Experimental Setup Long-Term Cultivation—2000-L Tumble Tanks

P. palmata was cultivated over a period of 3 years (2020–2022). At the beginning of the experiment, approximately 3.1 ± 0.2 kg of fresh *P. palmata* were placed in two 2000 L tanks with an illuminated surface of 3.14 m^2 each, resulting in an algal biomass density of 0.99 ± 0.07 g fresh weight (fw) L^{-1} . Seaweed density was kept constant by weighing biomass every two months and harvesting excess biomass to minimize the self-shading of seaweed thalli. Tumbling of seaweeds in the 2000 L tanks was ensured by aeration

using a centralized air injection and air pump (HAP 100, Raoping, Guangdong, China), releasing approx. $6.3 \text{ m}^3 \text{ h}^{-1}$ of air at a water height of 0.8 m. Air pumps were activated according to an automatic timer (Brennenstuhl Comfort-Line, Hugo Brennenstuhl GmbH & Co KG, Tuebingen, Germany), realizing a daily 12 h activation cycle from 07 a.m. to 07 p.m. The air injection served the movement of algae thalli to the exposed water surface, according to [24]. No artificial light was provided during the study. The 2000 L tumble tanks were covered by 1 cm thick transparent polycarbonate plates (Doppelstegplatten, S&V Stegplattenversand GmbH, Gelsenkirchen, Germany) with a light transmission rate of 82%, resulting in a reduced PAR rate on the water surface of the tank. Temperature and PAR (photosynthetically active radiation) were measured every 2 h using a data logger (HOBO Pendant MX2002, Metro GmbH, Düsseldorf, Germany) floating on the water surface in a third tank without cooling. To keep the temperature of the cultivation medium at an optimal temperature range between 12–14 °C for the cultivation of *P. palmata* [25], a cooling unit (Titan 6000, Aqua Medic, Bissendorf, Germany) was included in the cleaning circuit of the culture medium per tank. However, as the cooling unit only prevented an increase in the temperature in the summer months, lower temperatures during winter occurred.

As a nutrient supply, Provasoli Enrichment (PE) was provided once a week using a peristaltic pump (MP2-B, MicroDos Ltd., Rieti, Italy). PE was prepared according to the recipe given by [26]; however, the PE used did not contain Tris buffer and was used in tenfold concentration in order to avoid a decrease in salinity of the artificial medium due to long-term lack of medium replacement.

2.4. Experimental Setup Batch Tests—2-Liter Beakers

Prior to the beginning of the batch tests, diseased *P. palmata* thalli had been pre-incubated in a 160 L polyethylene tank for two weeks to eliminate the possibility of acclimation processes during the experiments. Here, the artificial conditions were a pH of 8.2, with 2 mL PE L⁻¹ cultivation medium per week (equals $1 \times \text{PE}$), a photon flux density of approx. $150 \pm 8 \mu\text{mol photons m}^{-2} \text{ s}^{-1}$ measured at the water surface and $13 \pm 1 \text{ }^\circ\text{C}$ as temperature of the medium. Fresh biomass density was approx. $2.35 \pm 0.42 \text{ g fw L}^{-1}$.

To study the effect of different cultivation conditions on the diseased thalli of *P. palmata*, tests were conducted using 2 L glass beakers (Simax Beaker, Kavalirglass A.S., Praha, Czech Republic). Three randomly selected, visibly diseased thalli were placed in each glass beaker filled with 1.7 L of artificial seawater medium. Every test group (V1-V6) was in triplicate. Tumbling of algae in the glass beakers was provided via glass tubes attached to an air pump (HAP 100, Raoping, Guangdong, China) supplying approx. $0.27 \text{ m}^3 \text{ h}^{-1}$ of air. Cold-white fluorescent tubes (Master TL-D Super 80, Osram, München, Germany) were used for the irradiation of beakers. Air pumps were activated in accordance with the automated 24-h light-dark cycle of 12:12 h. The culture medium was kept constant at 13 °C using a water chiller (Hailea HC-250A, Raoping, Guangdong, China). Photon fluence rate (PFR) was determined at the beginning of each test by measuring PFR on the water surface in the center of each beaker using a photon meter (LI-192, LI-190R, Li-Cor, Lincoln, NE, USA). Temperature and pH were measured every 10 min using a pH-temperature logger (Hobo Pendant pH-Temp, Metrics GmbH, Hagen, Germany). At the beginning and the end of each test run, the number of green/white spots and galls on the thalli were manually counted column by column from the frond base to the tips of the thalli. Measurement of the diameter of spots was performed using a ruler (Figure 1). Already formed holes were not counted.

Test conditions included pH levels of 7.5 and 9.1, different nutrient levels of $1 \times \text{PE}$ (2 mL PE per L⁻¹) and $3 \times \text{PE}$ (6 mL PE L⁻¹), different biomass densities of $4.85 \pm 0.47 \text{ g fw L}^{-1}$ compared to $2.35 \pm 0.33 \text{ g fw L}^{-1}$. Each test had a duration of 4 weeks and was performed at three different photon flux densities of 50 ± 7 , 150 ± 8 , $250 \pm 19 \mu\text{mol photons m}^{-2} \text{ s}^{-1}$ (Table 1). Regarding the test of different pH conditions, a combined pH meter and pH controller (pH 201, OCS.tec GmbH Co& KG, Neuching, Germany) was used to measure the pH every 10 min. To increase or to decrease the pH to the required level of 9.1 or 7.5 respectively,

the cultivation medium was fed with 10% NaOH or 10% HCl (Carl Roth GmbH & Co. KG., Karlsruhe, Germany) respectively, using peristaltic pumps (MP2-B, MicroDos Ltd., Rieti, Italy), which were electrically operated by the pH controller. As the control group, three diseased thalli of *P. palmata* were placed in glass beakers using the culture conditions of the incubation period in each respective test run: pH-level 8.2, $1 \times \text{PE}$, $2.35 \pm 0.33 \text{ g fw L}^{-1}$, with photon flux densities according to the specific test run.

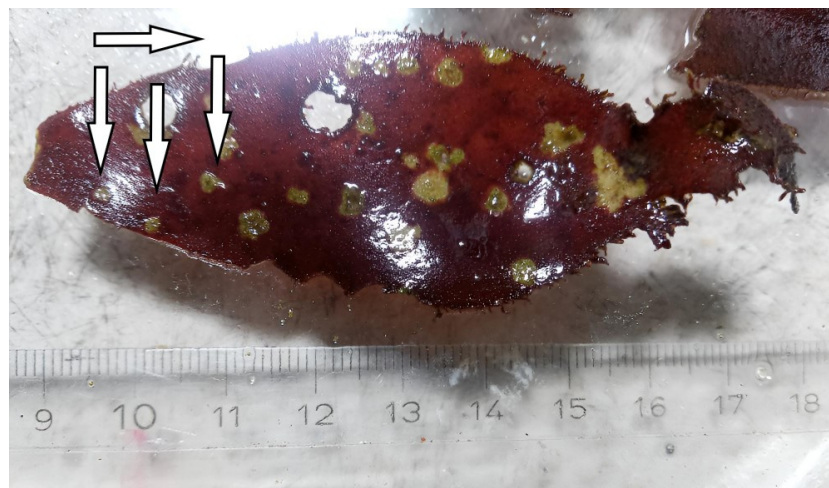


Figure 1. Direction of manual counting (white arrows) and measuring of spots column by column from the frond base to the tip of the thalli; holes were not counted.

Table 1. Batch test of 2 L beakers with test groups (V1–V6) and control. Control and tests were performed under photon flux densities of 50, 150, and $250 \mu\text{mol photons m}^{-2} \text{ s}^{-1}$. Test parameters included pH of 7.5 and 9.1, biomass density of $4.85 \pm 0.47 \text{ g fw L}^{-1}$ and $2.35 \pm 0.33 \text{ g fw L}^{-1}$, as well as nutrient levels of 1-time and 3-times PE. Each test was performed in triplicate.

Tested at PAR of 50, 150, and $250 \mu\text{mol m}^{-2} \text{ s}^{-1}$	pH-Level			Biomass Density [g fw L^{-1}]		Nutrients Supply (PE)	
	7.5	8.2	9.1	2.35 ± 0.33	4.85 ± 0.47	$1 \times \text{PE}$	$3 \times \text{PE}$
control		x		x		x	
V 1	x			x		x	
V 2			x	x		x	
V 3			x		x	x	
V 4			x		x		x
V 5	x				x		x
V 6	x			x			x

2.5. Microscopy Analysis

Light and fluorescence microscopy was conducted on *P. palmata* thalli fixed in 4% paraformaldehyde (first batch; date of harvest: March 2021) and 2.5% glutaraldehyde (second batch; date of harvest: January 2022). The fixed algal material was hand-cut in semi-thin transverse sections using razor blades. Bright-field and fluorescence observations (FITC filter Leica L5, Leica Biosystems Nussloch GmbH, Nußloch, Germany) were performed on an inverted fluorescence microscope (Leica DMI 8), and images were taken with a digital camera (Leica DMC 4500, Leica Biosystems Nussloch GmbH, Nußloch, Germany).

2.6. Chlorophyll Fluorescence Analyses

To assess the possible effects of an infection of *P. palmata* on the photosynthetic efficiency and on the fluorescence quenching of the thalli, chlorophyll fluorescence analyses (PAM-2000, Heinz Walz GmbH, Effeltrich, Germany) were conducted only on randomly selected thalli of *P. palmata* in the 2000 L tanks. Fluorescence analyses were conducted on

diseased areas, apparently healthy thalli, and healthy tissue in the direct vicinity (perimeter of 1–1.5 cm) of a diseased area. Rapid light curves (RLCs) were established for PFR ranges from 0 μmol to 363 $\mu\text{mol m}^{-2} \text{s}^{-1}$. After 30 min of dark acclimation, the initial fluorescence signal (F_0) and the maximal fluorescence of the dark-acclimated sample (F_m) were measured [27]. Based on the variable fluorescence F_v ($F_v = F_m - F_0$) and F_m , the potential maximum photochemical efficiency, which equals the potential maximum quantum yield of electron flow through PS II, was calculated as F_v/F_m [28]. The actual or effective quantum yield of electron flow through PS II ($Y(\text{II})$) was calculated as

$$Y(\text{II}) = (F_m' - F)/F_m'$$

where F_m' was the maximal fluorescence signal after a short (0.8 s) saturating pulse, and F was the actual fluorescence signal of continuously irradiated samples. The actual photosynthetic electron transport rate (ETR) was determined as

$$\text{ETR} = \text{PFR} \times Y(\text{II}) \times 0.5 \times \text{AF}$$

where AF (set to 0.57 according to [29]) was the incident light conversion efficiency of phototrophs [30–32]. The RLCs were analyzed according to [33] using the equation described by [34]. The following three parameters were derived from the fitted RLCs: maximum electron transport rate (ETR_{max}), the initial slope of light curves (alpha), which reflects the maximum light harvesting efficiency, and PFR at which ETR was light saturated (I_k), i.e., the ratio of ETR_{max} to alpha.

In addition, quantum yields of regulated ($Y(\text{NPQ})$) and non-regulated ($Y(\text{NO})$) non-photochemical energy dissipation of PS II were calculated according to [35] as

$$Y(\text{NPQ}) = (F/F_m')/(F/F_m) \text{ and } Y(\text{NO}) = F/F_m$$

2.7. Statistics

Data of fluorescence parameters $Y(\text{II})$, $Y(\text{NPQ})$, $Y(\text{NO})$ as well as ETR_{max}, E_k , alpha of infected and healthy tissue as well as tissue in the vicinity of an infection were statistically evaluated regarding the differences of the means with a confidence interval of 95%. A univariate ANOVA (Tukey test, $p < 0.05$) was used for the statistical analysis of each respective health status of a thalli (healthy, infected, and vicinity of an infection) and between the different health statuses using Origin 8G (OriginLab Corp., Northampton, MA, USA). Data on the size of spots under different cultivation conditions were tested using a two-sample F-test to test the two populations at the start and end of each test group regarding homogeneity. A paired sample T -test was used to test data for significant differences with a confidence interval of 95% regarding the size of spots and galls between the start and end of each test run in each test group. Data on changes in the number of spots and galls were not tested statistically.

3. Results

3.1. Temporal Occurrence and Changes in the Phenotype of *P. palmata* during Long-Term Cultivation

P. palmata was cultivated over a time period of 2 years, whereas the first visual indicators of a possible disease were detected in October/November 2020, one year after the beginning of cultivation in tumble tanks. Phenotypic changes were first visible as randomly shaped, but mostly circular shaped galls with a diameter of approx. 1–2 mm on the thalli (Figure 2d, right arrow). However, some thalli showed only homogeneous green spots of approx. 0.5–2 mm in diameter and no galls (Figure 2d, left arrow) as a first visual indicator of a disease. With a time of approx. 1–2 months, the galls increasingly developed into flat or sunken structures (Figure 2c), with greenish–white spots forming in the center of the galls, whereas the green spots increased in size (Figure 2b,e). In general, the galls and green spots were located randomly on the surface of the thalli. There was no clustering

at peripheral areas of the thalli. In later stages, the green spots or greenish–white areas extended and increasingly formed white circular or randomly shaped plaques of 1 cm or above (Figure 2b). In the final stage, the tissue within the white plaque was physically weakened, assumingly by the tumble cultivation, and finally disrupted, forming holes (Figure 2a). The thalli remained intact as long as the holes were small and not located near the peripheral area. In this case, epiphytes were occasionally growing on the border areas of the holes. If the damaged and disrupted area was large, a complete disruption of the thallus would result. An estimated 30% of the basic population (0.9 ± 0.19 kg fw) were infected during peak periods (winter/autumn) and ultimately lost to further cultivation.

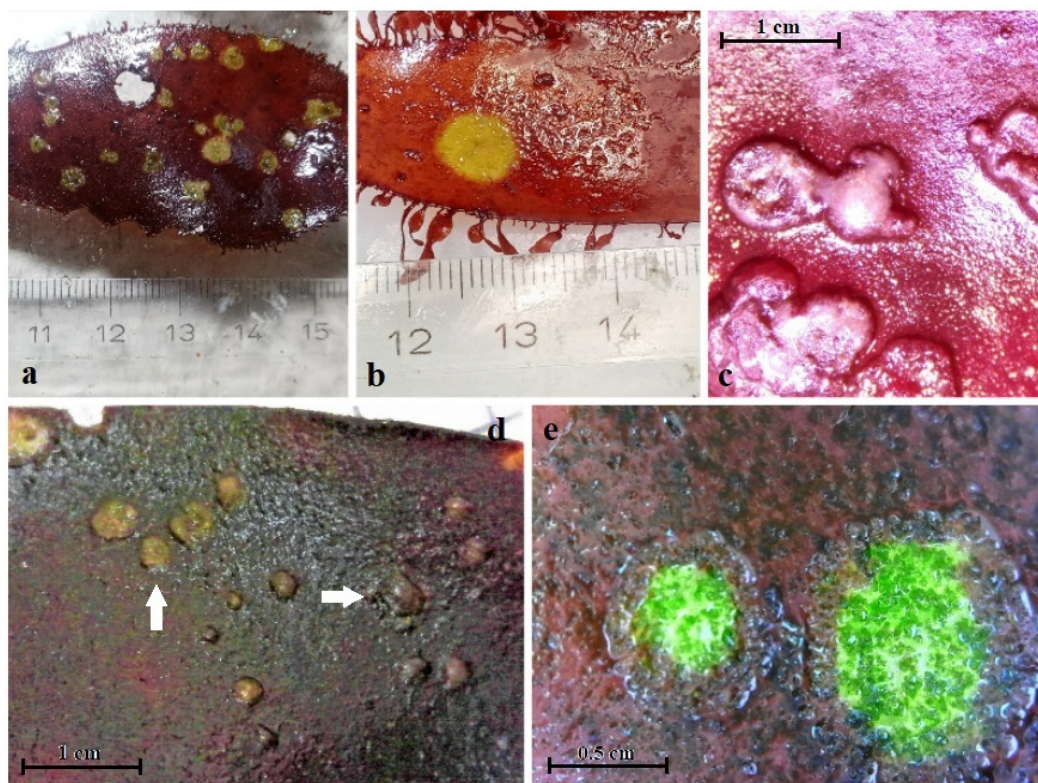


Figure 2. Phenotypic changes of *P. palmata*; (a) formation of holes as final stage; (b) greenish–white spots; (c) galls developing into flat or sunken structures; (d) first visual indicator as randomly shaped, but mostly circular shaped galls (right arrow) or as homogeneous green spots (left arrow); (e) greenish–white spots in the center of the galls or flat structures.

During the two years of cultivation (Figure 3), a visible increase in plaque formation on the thalli of *P. palmata* was detected repeatedly from October to December. The frequency of detected phenotypic changes (galls, green and white spots) increased until March/April. However, it was not documented whether the quality of the different symptoms changed from one year to the next. In both years in which infection was detected, galls, green and white spots, and perforated thalli were detected as the final state of the disease. Furthermore, the visibly affected thalli were discarded into separate tumble tanks. With the end of spring, the frequency of detected diseased thalli decreased and was minimal during the summer months. During summer months, the detected minimal frequency of disease patterns was approx. 2.3% of total biomass (0.07 ± 0.011 kg fw). Furthermore, during the summer months, the perforations, as the final state of the disease, showed a healthy rim and no signs of an area increase.

Figure 4 shows the temperature profile of the untreated/ uncooled cultivation medium (green dotted line) and the temperature range maintained by the cooling unit (grey shaded area) during the time period of the observed changes in the phenotypical appearance of *P. palmata* in the long-term cultivation vessels.

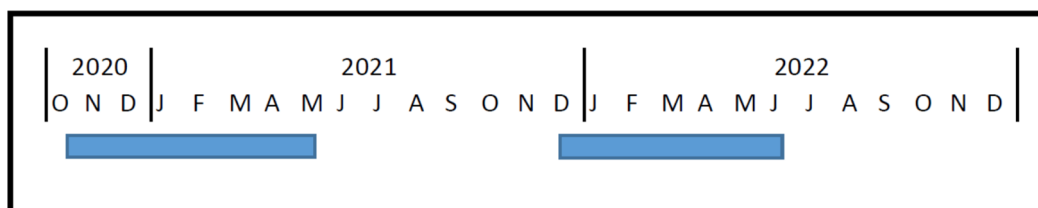


Figure 3. Time period of observed changes in the phenotypical appearance of *P. palmata* during approx. 2 years of tank cultivation; vertical lines indicate the turn of the years; blue bars indicate time periods of increased frequency of disease pattern.

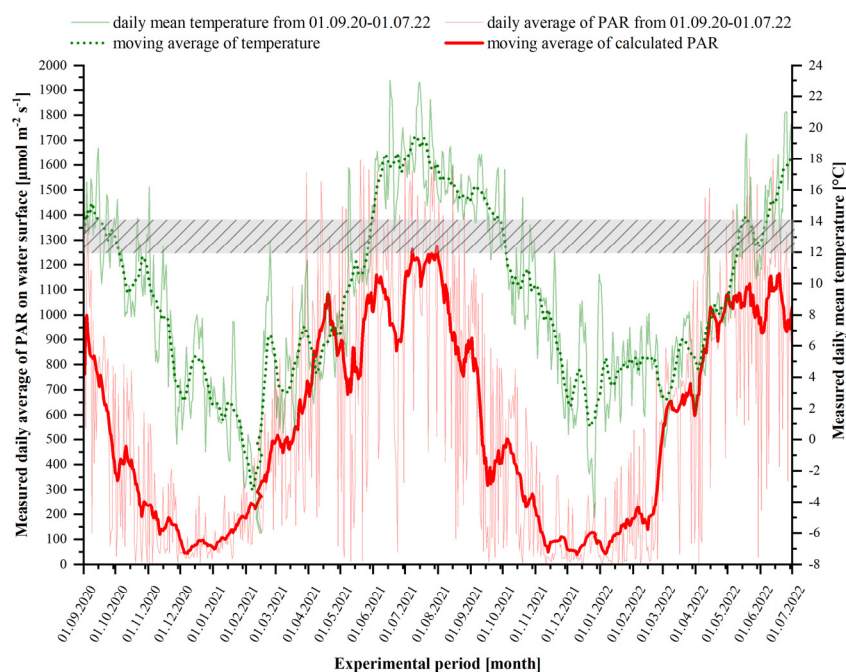


Figure 4. Representation of daily mean temperature (light green line) and moving average of daily mean temperature (green dotted line) as well as daily average PAR profile (light red line) and moving average of daily PAR (red line) during the experimental period from 1 September 2020 to 1 July 2022 measured in an outside tanks; optimal temperature range for *P. palmata* cultivation (grey shaded area) of 12–14 °C.

3.2. Effects of Varying Cultivation Conditions on Infection of *P. palmata*

To analyze the possible effect of different cultivation conditions on the propagation behavior of diseased areas, tests were performed at photon fluence densities of 50, 150, and 250 $\mu\text{mol photons m}^{-2} \text{s}^{-1}$. Different cultivation conditions, which included varying pH conditions (pH 7.5 in test group V1, V5, V6 vs. pH 9.1 in test group V2, V3, V4), different nutrient levels (1 \times PE vs. 3 \times PE) and different biomass densities ($\approx 4.85 \pm 0.47 \text{ g fw L}^{-1}$ vs. $\approx 2.35 \pm 0.33 \text{ g fw L}^{-1}$) were tested regarding their effect on the size (Figures 5–7) and number of infections (Table 2). Data of plaque size at 50 $\mu\text{mol photons m}^{-2} \text{s}^{-1}$ (Figure 5) showed a significant ($p < 0.05$) increase in the size of spots in test groups V2 and V3 between the beginning and end of the test run. Test groups V2 and V3 were both characterized by an increased pH and a normal level of nutrients, whereas biomass density was normal in V2 and high in V3. At 150 $\mu\text{mol photons m}^{-2} \text{s}^{-1}$ (Figure 6), data of changes in plaque size showed no significant differences within the test runs, whereas, at 250 $\mu\text{mol photons m}^{-2} \text{s}^{-1}$ (Figure 7), plaque size increased significantly for test groups V2, V3, V5, and V6 between the beginning and end of the test run. In this regard, test groups V5 and V6 were both characterized by a decreased pH and a high level of nutrients. Biomass density was high in V5 and normal in V6. In general, diseased *P. palmata* thalli tested at pH 9.1 showed

an overall loss in firmness of *P. palmata* tissue, especially the infected areas, as well as tissue in the direct vicinity of the plaques, which became softer and tended to break more easily. At $250 \mu\text{mol photons m}^{-2} \text{s}^{-1}$, bleaching of all thalli was visible in all test setups, accompanied by a noticeable increase in the size of galls and green spots, yet without an increase in the number of infections.

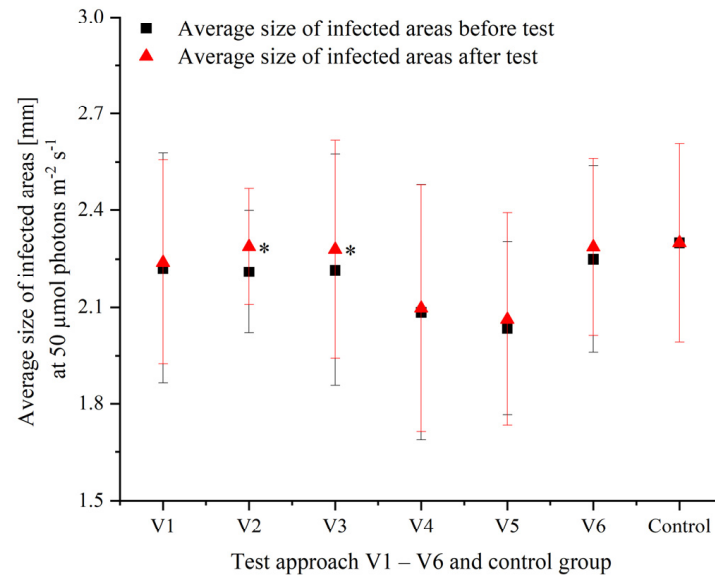


Figure 5. Average size [mm] with the standard deviation of infected areas at the beginning (black square) and end (red triangle) of the test runs at $50 \mu\text{mol photons m}^{-2} \text{s}^{-1}$; “*” represents significantly different sizes of infections in a specific test group after the test run.

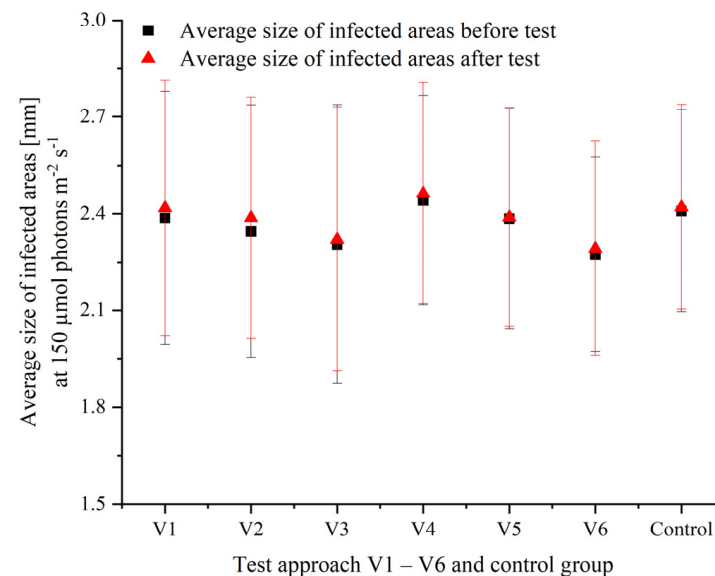


Figure 6. Average size [mm] with the standard deviation of infected areas at the beginning (black square) and end (red triangle) of the test runs at $150 \mu\text{mol photons m}^{-2} \text{s}^{-1}$.

Regarding the number of infections between the beginning and the end of the test runs (Table 2), a notable, however not statistically evaluated, increase was detected at $50 \mu\text{mol photons m}^{-2} \text{s}^{-1}$, counting 11 infections on thalli of *P. palmata*. No test group showed a particularly apparent increase in spots. In comparison, at $150 \mu\text{mol photons m}^{-2} \text{s}^{-1}$ as well as at $250 \mu\text{mol photons m}^{-2} \text{s}^{-1}$, the number of new infections in all test runs counted to 5. Thus, according to our observations, small green spots were more frequently detectable under low-light conditions.

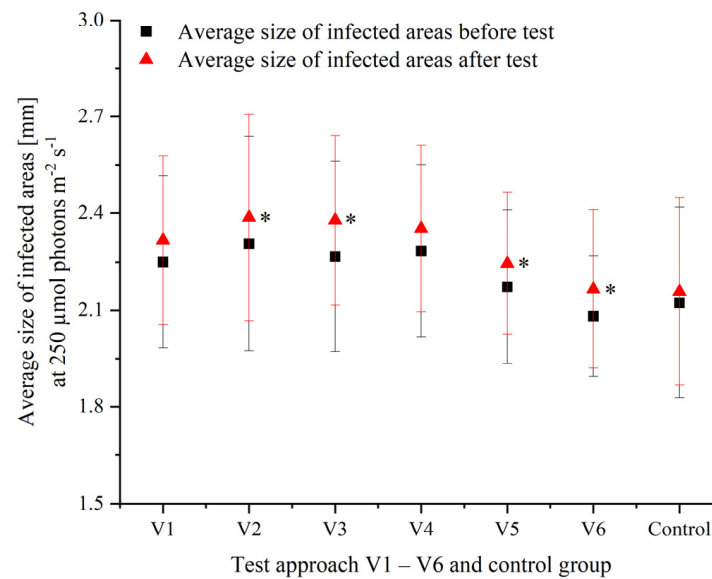


Figure 7. Average size [mm] with the standard deviation of infected areas at the beginning (black square) and end (red triangle) of the test runs at 250 $\mu\text{mol photons m}^{-2} \text{s}^{-1}$; “*” represent significantly different sizes of infections in a specific test group after the test run.

Table 2. Counted the number of infections in each test group and control (Contr.) at three different photon fluence rates (50, 150, and 250 $\mu\text{mol photons m}^{-2} \text{s}^{-1}$) and the number of additional infections that appeared during the test period. Every test was in triplicate (group X.1–X.3) containing three infected thalli each (X, Y, Z). Infections were counted at the start and the end of the test period.

Test Group	Number of infections at PAR 50		Additional Number of Infections	Number of Infections at PAR 150		Additional Number of Infections	Number of Infections at PAR 250		Additional Number of Infections
	Start	End		Start	End		Start	End	
V1.1	6,8,3	7,8,3	1	5,6,8	5,6,8	0	7,4,5	7,4,5	0
V1.2	4,5,5	4,5,5	0	6,7,6	6,7,6	0	3,5,5	4,5,5	1
V1.3	5,5,6	5,6,6	1	5,9,4	5,10,4	1	7,5,8	7,5,8	0
V2.1	2,8,4	2,9,4	1	8,6,9	8,6,9	0	4,5,8	4,5,8	0
V2.2	4,6,5	4,6,5	0	8,3,2	9,3,2	1	9,6,4	9,7,4	1
V2.3	5,5,8	5,6,8	1	6,4,4	6,4,4	0	4,2,9	4,2,9	0
V3.1	7,8,3	7,9,3	1	6,7,7	6,7,7	0	4,8,5	4,8,5	0
V3.2	5,6,4	5,6,5	1	7,5,9	7,5,9	0	4,5,7	4,5,7	0
V3.3	3,4,3	3,4,3	0	4,6,7	4,7,7	1	4,4,7	5,4,7	1
V4.1	9,4,2	10,4,2	1	5,7,5	5,7,5	0	4,8,5	4,8,5	0
V4.2	4,7,4	4,7,4	0	6,5,8	6,5,9	1	7,3,8	7,3,9	1
V4.3	7,5,8	7,6,8	1	6,7,3	6,7,3	0	5,6,7	5,6,7	0
V5.1	4,7,5	4,7,5	0	10,7,8	10,7,8	0	8,7,8	8,7,8	0
V5.2	7,7,9	7,7,9	0	4,8,5	4,8,5	0	5,7,5	5,7,5	0
V5.3	5,2,7	6,2,7	1	6,6,4	6,6,4	0	3,7,8	3,7,8	0
V6.1	6,3,4	6,3,4	0	4,9,9	4,9,9	0	5,4,6	5,4,6	0
V6.2	8,3,5	9,3,6	2	11,8,6	12,8,6	1	7,6,7	7,6,8	1
V6.3	3,3,6	3,3,6	0	6,9,6	6,9,6	0	5,6,4	5,6,4	0
Contr. 1	4,7,8	4,7,8	0	7,9,8	7,9,8	0	7,4,6	7,4,6	0
Contr. 2	8,7,3	8,8,3	1	4,7,5	4,7,5	0	8,5,6	8,5,6	0
Contr. 3	4,9,5	4,9,5	0	9,4,7	9,4,7	0	5,6,6	5,6,6	0

3.3. Effects of Infection on Photosynthetic Activity and Fluorescence Quenching of *P. palmata*

PAM measurements of healthy thalli, visibly not diseased tissue in the direct vicinity of a diseased area, and infected greenish–white areas were tested regarding photosynthetic activity. Measurements showed a slight, but not significant, decrease in the rate of electron transport through PSII (ETR_{max}) and the efficiency of electron transport (alpha) in the

tissue around a diseased area in comparison to healthy tissue. In comparison, no significant difference in the saturation irradiance (E_K) was detected between healthy *P. palmata* tissue and tissue in the vicinity of the disease. However, all photosynthetic parameters of diseased tissue were significantly ($p < 0.05$) reduced in comparison to healthy tissue as well as to parameters of tissue in the vicinity of the diseased area (Table 3).

Table 3. Mean values of maximum electron transport through PSII (ETR_{max}), saturating irradiance (E_K), and efficiency of photosynthetic electron transport (α) of healthy tissue, tissue area in the direct vicinity of infection, and infected areas of *P. palmata*; 5 different measurements at healthy tissue, infected tissue, and tissue around the infected area ($n = 5$); “*” represents significant differences ($p < 0.05$) between values of healthy tissue and infected tissue as well as between healthy tissue and tissue in the vicinity of an infection.

	ETR_{max}	Healthy Tissue <i>alpha</i>	E_K
Mean value	23.03	0.187	123.45
SD	2.51	0.010	16.75
	Tissue around the infected area		
	ETR_{max}	<i>alpha</i>	E_K
Mean value	21.19	0.173	123.47
SD	1.77	0.018	10.71
	Infected tissue		
	ETR_{max}	<i>alpha</i>	E_K
Mean value	12.80 *	0.138 *	92.91 *
SD	1.45	0.012	5.65

The actual quantum yield of electron transport through PSII ($Y(II)$) was significantly decreased ($p < 0.05$) in the infected tissue in comparison to areas in the direct vicinity of infection and to healthy thalli for the whole PAR range (Figure 8). Significant differences were also identified for $Y(II)$ in the lower PAR range ($0\text{--}116 \mu\text{mol photons m}^{-2} \text{s}^{-1}$) between tissue in the direct vicinity of the infection and healthy tissue. Similarly, the nonregulated non-photochemical quenching ($Y(NO)$) was significantly increased ($p < 0.05$) only in the lower PAR range ($0\text{--}75 \mu\text{mol photons m}^{-2} \text{s}^{-1}$) in infected areas in comparison to the healthy areas and healthy areas in the vicinity of infection (Figure 9). The regulated non-photochemical quenching ($Y(NPQ)$) of infected tissue was significantly decreased ($p < 0.05$) nearly in the whole tested PAR spectrum ($43\text{--}363 \mu\text{mol photons m}^{-2} \text{s}^{-1}$) compared to $Y(NPQ)$ of healthy tissue. $Y(NPQ)$ of tissue in the direct vicinity of an infection compared to $Y(NPQ)$ of healthy tissue was lowered and significantly reduced ($p < 0.05$) in the higher PAR range from 112 to $363 \mu\text{mol photons m}^{-2} \text{s}^{-1}$ (Figure 10). Thus, the regulated heat dissipation, which is a regulated dissipation of overexcitation of reaction centers, is also mitigated in the vicinity of the infected region.

3.4. Preliminary Microscopy Investigation of Diseased *P. palmata* Thalli

Macroscopic initial observations of *P. palmata* material showing signs of disease revealed several phenotypes: wart-like structures, areas of thickened *P. palmata* tissue (cf. Figure 2), and green spots. Those regions were subsequently investigated via microscopy and compared to control *P. palmata* material without any visual indicators of disease. Areas of the thalli showing spots and warts were significantly thicker compared to thalli sections without any sign of disease (Figure 11a,b). Cross-sections revealed the presence of opaque grey or brownish medulla cells in the thickened parts of the *P. palmata* thallus (Figure 11b). Those cells were highly prominent in number and restricted to the diseased parts of the *P. palmata* thallus (Figure 11c). In some cases, they were also found in the close vicinity of the diseased part. Healthy areas of the *P. palmata* thallus showed clear medulla cells (Figure 11d), as in the case of healthy *P. palmata* material. The opaque medulla

cells showed green autofluorescence, which was absent from healthy medulla cells and indicated intracellular granular structures of various sizes (Figure 11e).

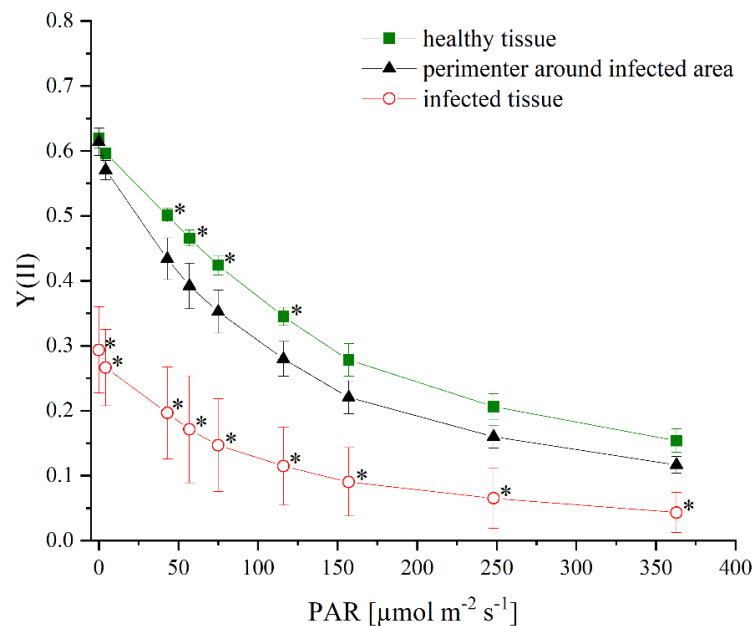


Figure 8. Mean values of effective quantum yield of electron transport through PSII ($Y(II)$) with increasing irradiance of infected *P. palmata* tissue (red circle) in the vicinity of infected tissue (black triangle) and visibly healthy tissue (green square); “*” at red circles represent significant differences ($p < 0.05$) of infected thalli in comparison to healthy tissue and to tissue in the vicinity of an infection; “*” at green squares represent significant differences ($p < 0.05$) of healthy thalli in comparison to tissue in the vicinity of an infection.

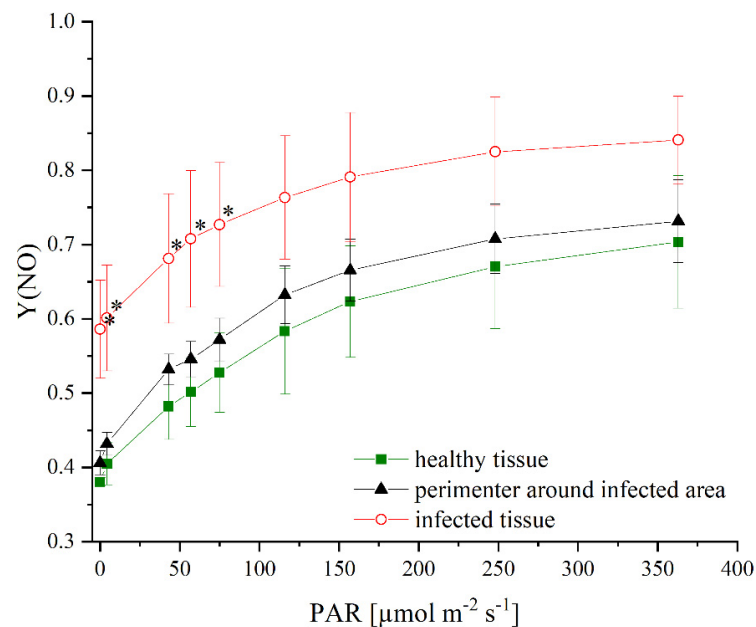


Figure 9. Mean values of non-regulated non-photochemical quenching ($Y(NO)$) with increasing irradiance of infected *P. palmata* tissue (red circle), in the vicinity of infected tissue (black triangle) and visibly healthy tissue (green square); “*” represent significant differences ($p < 0.05$) of infected thalli in comparison to healthy tissue and to tissue in the vicinity of an infection.

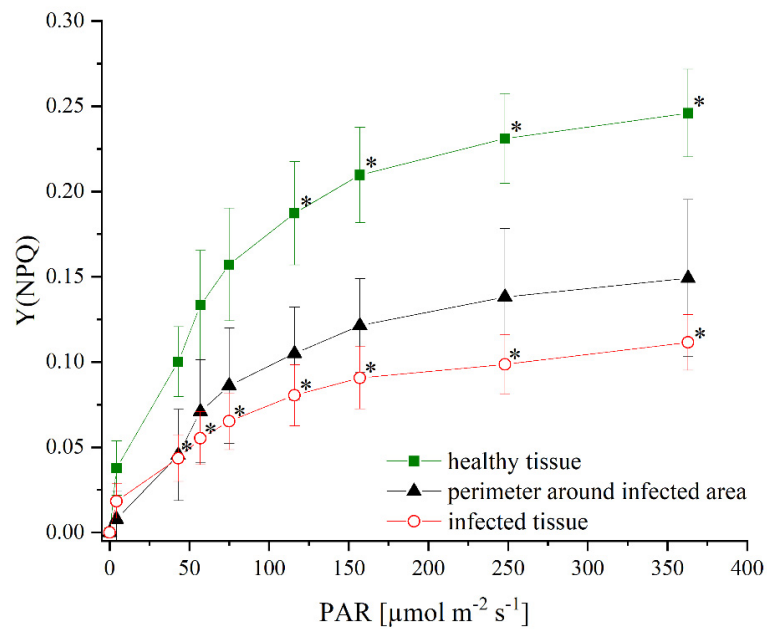


Figure 10. Mean values of regulated non-photochemical quenching Y(NPQ) with increasing irradiance of infected *P. palmata* tissue (red circle) in the vicinity of infected tissue (black triangle) and visibly healthy tissue (green square); “*” at red circles represent significant differences ($p < 0.05$) of infected thalli in comparison to healthy tissue; “*” at green squares represent significant differences ($p < 0.05$) of healthy thalli in comparison to tissue in the vicinity of an infection.

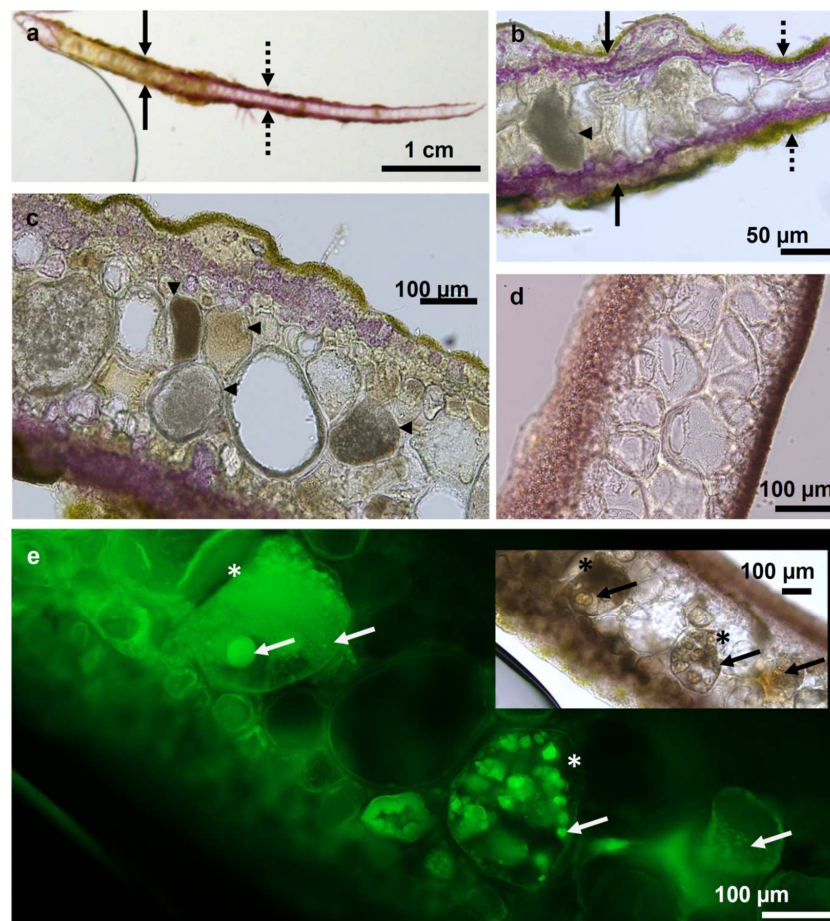


Figure 11. Microscopy of diseased *P. palmata* thalli: Semi-thin transverse section of a diseased area of the *P. palmata* thallus (a,b); The diseased area appears greenish and thickened (arrows) compared to

the adjacent thinner region without any visual abnormalities (dotted arrows); In diseased areas of the thallus medulla cells appear opaque (arrowheads; b,c); The medulla cells in healthy parts of the thallus show clear medulla cells (d); Green autofluorescence of opaque medulla cells (asterisk; e); Granular units can sometimes be observed within those cells (arrows).

4. Discussion

The present study was motivated by the appearance of phenotypical changes after the first year of a land-based cultivation set-up of the red alga *P. palmata*. Although the efforts to link the observed phenotypical changes in *P. palmata* to a pathogenic organism did not yet lead to an identification, we present here a preliminary macroscopic description, test results of chlorophyll fluorescence analyses, and experimental results to determine the effect of changing culture conditions on pathological symptoms, which should be amended by future electron microscopy analysis. However, as the identification of the cause of the phenotypical changes is still pending, the test conditions focused on the mitigation of the symptoms of infected thalli.

Although diseases and pests of seaweeds have been known for at least 100 years [36], the scientific knowledge about pathogens, possible causes, and treatments remains incomplete [14]. However, phenotypical changes in seaweed, as well as declining yields of produced seaweed, are known to be caused by diseases and pests [11,14,37] or by abiotic and external changes in the cultivation conditions [38]. Pests like grazers, epiphytes, and biofoulers can cause the detected seaweed changes and crop losses [39] or be the consequence of a previous impairment of macroalgae [18,39,40]. Diseases caused by viruses, bacteria, fungi, or endophytes can also be responsible for phenotypical changes in seaweed or production losses [18,41,42]. Additionally, climatic changes might stimulate the vulnerability of seaweed to disease agents and pests [14,37].

Regarding the detected pathological changes of *P. palmata*, it was shown that observed cell proliferation of cortical and medullary tissue led to the formation of galls and cushion-like structures similar to hyperplasia symptoms of terrestrial plants [14,37]. These symptoms were sometimes followed by necrosis of the proliferated areas and adjacent tissue, resulting in the formation of holes. According to [37], it can be assumed that these symptoms, which are remotely similar to the pathological symptoms of the “red rot disease”, “chytrid blight”, or “Anaaki disease” [14], might be caused by bacterial pathogens or oomycetes as found for the red algae *Porphyra yezoensis* [43–45]. However, in addition to the formation of galls, green and white spots were detected on the thallus of *P. palmata*. Similar pathological phenomena were found in *P. yezoensis*, *P. tenera*, and *P. dentata*, caused, however, by a chloroplast virus [10], resulting in a disease known as “green spot rot” [14]. Regarding the appearance of green spots, it was found that the marine fungi *Mycaureola dilseae* causes similar circular necrotic lesions of the algal tissue in *Dilsea carnosa* as found within this study [46]. Another case is described by [47], where a pathogenic bacteria is the cause of a disease in which decaying spots form on the thallus of *Undaria pinnatifida*.

Based on these findings, it might be possible that different and independent factors led to the detected symptoms of galls, cushions, and green and white spots. However, the formation of galls and necrosis might also be caused by obligatory or facultative algal endophytes [37]. In this regard, a simultaneous or secondary infection/colonization of fractures or separation areas by pathogens cannot be excluded, which means that the cause-and-effect relation might be more complicated to clarify [48]. Furthermore, similar to the results of [17] on the red algae *Kappaphycus alvarezii* and considering the detected seasonal variability of the pathological changes of *P. palmata*, it can be assumed that an epiphytic infection might also take part in causing the symptoms [49]. In this regard, [17] showed a relationship between abiotic factors like salinity and temperature and the occurrence of pathological changes in *K. alvarezii*. Accordingly, our study might indicate an interrelation between seasonality and the occurrence of the pathogen. Therefore, specific abiotic factors

and, more specifically, changing abiotic factors might lead to a dysbiosis of the algal microbiome and a proliferation of virulent agents [50]. Thus, in summer, the occurrence of pathological changes in *P. palmata* decreased and increased in the winter. As salinity and nutrient supply were unchanged during the year, light quantity, quality, and temperature might be partly responsible for the detected changes. Furthermore, according to [17] and [51], drastic changes in these abiotic factors can trigger or stimulate the increase of symptoms of bacterial and endophytic infections. Similarly, quickly altering environmental conditions could also lead to stressful abiotic conditions, which in turn might cause an overall weakened state of the seaweed.

In small-scale tests, we demonstrated a significant effect of light quantity on the size of the infected area. At low-light test conditions, the size of infected areas was significantly increased in test groups with an elevated pH and a normal nutrient supply. In comparison, in all the other test groups, regardless of pH and nutrient supply, the size of the infection remained unchanged. The test results under low-light conditions showed, in general, a notable, though not statistically evaluated, increase in the number of infections.

In comparison, under high-light conditions, the size of infected areas significantly increased as well, both in test groups with lowered and elevated pH and also in test groups with normal and increased nutrient supply. However, the number of infections under high-light conditions was notably decreased in comparison to low-light conditions. Thus, it can be assumed that low-light conditions might affect the number of infections, whereas high-light conditions might influence the size of infected areas. At medium-range light conditions, there was only a negligible increase in the size of infected areas in the control and all test groups—independently of the nutrient level or the tested biomass density. Additionally, there was a similarly low number of additional infections during the test period at medium-light conditions. Thus, it can be assumed that light quantity might be the most important factor for the propagation behavior of the infection, whereas the pH level might be secondary, nutrient level, and biomass density of minor relevance, similar to the findings of [52].

It seems that the observed increase and decrease of pathological symptoms of *P. palmata* in the 2000 L outdoor tanks might be due to seasonal changes in light quantity. Similarly, changes in light quality and temperature—though not tested within this study—could also influence the occurrence of pathological changes in *P. palmata* as described for *Fucus vesiculosus* [53].

The results of chlorophyll fluorescence measurements of the *P. palmata* clearly showed the photosynthetic damage of the diseased area in comparison to healthy thalli. Diseased areas showed a significant drop in the photosynthetic capacity (ETR_{max}) and light-harvesting efficiency (alpha) together with a decrease of photochemical quenching Y(II) and reduced regulated photoprotective mechanisms for energy dissipation Y(NPQ). Additionally, a significant increase of Y(NO) emphasized the reduced capacity of infected thalli of *P. palmata* to adequately use light energy either for photosynthesis or to dissipate light energy via regulated photoprotective processes [35,54]. In comparison, photosynthesis of tissue in the direct vicinity of a diseased area was only slightly reduced in comparison to the control group, hence pointing out the limited effect of the detected pathological changes on photosynthetic activity. Similarly, the quenching ability of tissue in the direct vicinity of a diseased area was slightly increased in the case of Y(NO) in comparison to healthy tissue, indicating only a slight effect of the disease on the non-regulated non-photochemical quenching ability of the surrounding tissue. However, the Y(NPQ) of the tissue in the direct vicinity of a diseased area was already significantly reduced in comparison to healthy tissue, suggesting an already existing effect of the unidentified pathogen on the regulated quenching capabilities of the surrounding area.

5. Conclusions

The investigation of abnormalities and phenotypical changes is of the utmost importance as part of the successful establishment of an economically feasible algal cultivation.

Pathological changes, as observed in *P. palmata* for over 2 years, lead not only to reduced photosynthesis but also to weakened tissue and ultimately to losing the cultivated seaweed. Cultivation tests, as well as observations, showed that, in particular, the light quantity was of primary importance for the propagation behavior of the infection, whereas the pH level might be of secondary, nutrient level, and biomass density of minor importance for the formation of galls and green spots. However, as no biomolecular tests were performed during this study, future examinations have to include molecular biological analyses to determine the agent responsible for the pathological changes. Additionally, more tests are needed to determine (a) a possible seasonality of the infection, as it remains unclear whether the proliferation of the pathogen might be stimulated via a specific abiotic factor, and (b) precise countermeasures in the cultivation procedure to avoid the propagation of the disease if they occur, as well as (c) measures to further lessen the symptoms of the disease if an infection occurs. In this context, a land-based cultivation facility might offer the advantage of limited varying abiotic factors compared to sea-based cultivation, which can facilitate the identification of the causative agent and the establishment of suitable prevention and treatment strategies.

Author Contributions: Conceptualization and methodology, S.S. and D.H.; laboratory analysis, M.S. and C.M.M.G.; data curation, S.S.; writing—original draft preparation, S.S., D.H. and M.S.; writing—review and editing, S.S., D.H. and M.S.; supervision, D.H. and C.M.M.G.; project administration, D.H.; funding acquisition for microscopic analysis, C.M.M.G. and M.S. All authors have read and agreed to the published version of the manuscript.

Funding: M.S. and C.M.M.G. were funded by GENIALG: GENetic diversity exploitation for Innovative macro-ALGal biorefinery: H2020-BG1-2016 and by GlobalSeaweed-STAR—Safeguarding the future of seaweed aquaculture in developing countries: UKRI GCRF (BB/P027806/1).

Institutional Review Board Statement: Not applicable.

Informed Consent Statement: Not applicable.

Data Availability Statement: The data presented in this study are available on request from the corresponding author.

Conflicts of Interest: The authors declare no conflict of interest.

References

1. Baghel, R.S.; Suthar, P.; Gajaria, T.K.; Bhattacharya, S.; Anil, A.L.; Reddy, C. Seaweed biorefinery: A sustainable process for valorising the biomass of brown seaweed. *J. Clean. Prod.* **2020**, *263*, 121359. [[CrossRef](#)]
2. Chung, I.K.; Beardall, J.; Mehta, S.; Sahoo, D.; Stojkovic, S. Using marine macroalgae for carbon sequestration: A critical appraisal. *J. Appl. Phycol.* **2011**, *23*, 877–886. [[CrossRef](#)]
3. Kumar, V.; Zozaya-Valdes, E.; Kjelleberg, S.; Thomas, T.; Egan, S. Multiple opportunistic pathogens can cause a bleaching disease in the red seaweed *Delisea pulchra*. *Environ. Microbiol.* **2016**, *18*, 3962–3975. [[CrossRef](#)] [[PubMed](#)]
4. Milledge, J.J.; Smith, B.; Dyer, P.W.; Harvey, P. Macroalgae-derived biofuel: A review of methods of energy extraction from seaweed biomass. *Energies* **2014**, *7*, 7194–7222. [[CrossRef](#)]
5. Prasedya, E.S.; Frediansyah, A.; Martyasari, N.W.R. Effect of particle size on phytochemical composition and antioxidant properties of *Sargassum cristaefolium* ethanol extract. *Sci. Rep.* **2021**, *11*, 17876. [[CrossRef](#)] [[PubMed](#)]
6. Wang, X.; Broch, O.J.; Forbord, S.; Handå, A.; Skjermo, J.; Reitan, K.I.; Olsen, Y. Assimilation of inorganic nutrients from salmon (*Salmo salar*) farming by the macroalgae (*Saccharina latissima*) in an exposed coastal environment: Implications for integrated multi-trophic aquaculture. *J. Appl. Phycol.* **2014**, *26*, 1869–1878. [[CrossRef](#)]
7. Pedro, M.; Garvetto, A.; Egan, S.; Gachon, C.M.M. The Reemergence of Phycopathology: When Algal Biology Meets Ecology and Biosecurity. *Annu. Rev. Phytopathol.* **2023**, *61*, 231–255.
8. Wang, G.; Shuai, L.; Li, Y. Phylogenetic analysis of epiphytic marine bacteria on Hole-Rotten diseased sporophytes of *Laminaria japonica*. *J. Appl. Phycol.* **2008**, *20*, 403–409. [[CrossRef](#)]
9. Kim, G.H.; Moon, K.-H.; Kim, J.-Y.; Shim, J.; Klochkova, T.A. A reevaluation of algal diseases in Korean *Pyropia* (*Porphyra*) sea farms and their economic impact. *Algae* **2014**, *29*, 249–265. [[CrossRef](#)]
10. Kim, G.H.; Klochkova, T.A.; Lee, D.J.; Im, S.H. Chloroplast virus causes green-spot disease in cultivated *Pyropia* of Korea. *Algal. Res.* **2016**, *17*, 293–299. [[CrossRef](#)]

11. Cottier-Cook, E.J.; Nagabhatla, N.; Badis, Y.; Campbell, M.; Chopin, T.; Dai, W.; Fang, J.; He, P.; Hewitt, C.; Kim, G.H.; et al. *Safeguarding the Future of the Global Seaweed Aquaculture Industry*; United Nations University (INWEH) and Scottish Association for Marine Science Policy Brief: Hamilton, ON, Canada, 2016; 12p, ISBN 978-92-808-6080-1.
12. Hurtado, A.Q.; Cheney, D.P. Propagule production of *Euclidean denticulatum* (Burman) Collins et Harvey by tissue culture. *Bot. Mar.* **2003**, *46*, 338–341. [[CrossRef](#)]
13. Pedrosa, A.A. Current status of Philippine seaweed industry. In Proceedings of the Regional Scientific Meeting on Attaining Sustainable Development Goals: Philippines Fisheries and Other Aquatic Resources 20/20, SMX Convention Center, Davao City, Philippines, 7 July 2017.
14. Ward, G.M.; Faisan, J.P., Jr.; Cottier-Cook, E.J.; Gachon, C.; Hurtado, A.Q.; Lim, P.E.; Matoju, I.; Msuya, F.E.; Bass, D.; Brodie, J. A review of reported seaweed diseases and pests in aquaculture in Asia. *J. World Aquacul. Soc.* **2019**, *51*, 815–828. [[CrossRef](#)]
15. Zambounis, A.; Strittmatter, M.; Gachon, C.M.M. Chronic stress and disease resistance in the genome model marine seaweed *Ectocarpus siliculosus*. *Aquat Bot.* **2013**, *104*, 147–152. [[CrossRef](#)]
16. Heath, S.E.; Knox, K.; Vale, P.F.; Collins, S. Virus Resistance Is Not Costly in a Marine Alga Evolving under Multiple Environmental Stressors. *Viruses* **2017**, *9*, 39. [[CrossRef](#)] [[PubMed](#)]
17. Vairappan, C.S.; Chung, C.S.; Hurtado, A.Q.; Msuya, F.E.; Bleicher-Lhonneur, G.; Critchley, A. Distribution and symptoms of epiphyte infection in major carrageenophyte-producing farms. *J. Appl. Phycol.* **2008**, *20*, 477–483. [[CrossRef](#)]
18. Loureiro, R.; Gachon, C.M.M.; Rebours, C. Seaweed cultivation: Potential and challenges of crop domestication at an unprecedented pace. *New Phytol.* **2015**, *206*, 489–492. [[CrossRef](#)] [[PubMed](#)]
19. Badis, Y.; Klochkova, T.A.; Strittmatter, M. Novel species of the oomycete *Olpidiopsis* potentially threaten European red algal cultivation. *J. Appl. Phycol.* **2019**, *31*, 1239–1250. [[CrossRef](#)]
20. Grote, B. Recent developments in aquaculture of *Palmaria palmata* (Linnaeus) (Weber & Mohr 1805): Cultivation and uses. *Rev. Aquac.* **2019**, *11*, 25–41.
21. Le Gall, L.; Pien, S.; Rusig, A.M. Cultivation of *Palmaria palmata* (Palmariales, Rhodophyta) from isolated spores in semicontrolled conditions. *Aquaculture* **2004**, *229*, 181–191. [[CrossRef](#)]
22. Mishra, V.K.; Temelli, F.; Oraikul, B.; Shacklock, P.F.; Craigie, J.S. Lipids of the red alga, *Palmaria palmata*. *Bot. Mar.* **1993**, *36*, 169–174. [[CrossRef](#)]
23. Kerrison, P.D.; Le, H.N.; Twigg, G.C. Decontamination treatments to eliminate problem biota from macroalgal tank cultures of *Osmundea pinnatifida*, *Palmaria palmata* and *Ulva lactuca*. *J. Appl. Phycol.* **2016**, *28*, 3423–3434. [[CrossRef](#)] [[PubMed](#)]
24. Bidwell, R.G.S.; McLachlan, J.; Lloyd, N.D.H. Tank cultivation of Irish moss, *Chondrus crispus* Stackh. *Bot. Mar.* **1985**, *28*, 87–97. [[CrossRef](#)]
25. Demetropoulos, C.L.; Langdon, C.J. Enhanced production of Pacific dulse (*Palmaria mollis*) for co-culture with abalone in a land-based system: Effects of stocking density, light, salinity and temperature. *Aquaculture* **2004**, *235*, 471–488. [[CrossRef](#)]
26. Berges, J.A.; Franklin, D.J.; Harrison, P.J. Evolution of an artificial seawater medium: Improvements in enriched seawater, artificial water over the last two decades. *J. Phycol.* **2001**, *37*, 1138–1145. [[CrossRef](#)]
27. Hanelt, D.; Huppert, K.; Nultsch, W. Photoinhibition of photosynthesis and its recovery in red algae. *Bot. Acta.* **1992**, *105*, 278–284. [[CrossRef](#)]
28. Schreiber, U.; Schliwa, U.; Bilger, W. Continuous recording of photochemical and non-photochemical chlorophyll fluorescence quenching with a new type of modulated fluorometer. *Photosynth. Res.* **1996**, *10*, 51–62. [[CrossRef](#)]
29. Beer, S.; Axelsson, L. Limitations in the use of PAM fluorometry for measuring photosynthetic rates of macroalgae at high irradiances. *Eur. J. Phycol.* **2004**, *39*, 1–7. [[CrossRef](#)]
30. Herppich, W.B.; Herppich, M.; Von Willert, D.J. Ecophysiological investigations on plants of the genus *Plectranthus* (Lamiaceae). Influence of environment and leaf age on CAM gas exchange and leaf water relations in *Plectranthus marrubioides*. *Flora* **1998**, *193*, 99–109. [[CrossRef](#)]
31. Herppich, W.B.; Herppich, M.; Tüffers, A.; Von Willert, D.J.; Midgley, G.F.; Veste, M. Photosynthetic responses to CO₂ concentration and photon fluence rates in the CAM-cycling plant *Delosperma tradescantioides* (Mesembryanthemaceae). *New Phytol.* **1998**, *138*, 433–440. [[CrossRef](#)]
32. Hanelt, D. Photosynthesis assessed by chlorophyll fluorescence. In *Bioassays, Advanced Methods and Applications*; Häder, D.P., Erzinger, G.S., Eds.; Elsevier: Amsterdam, The Netherlands, 2018; pp. 169–198.
33. Jassby, A.D.; Platt, T. Mathematical formulation of the relationship between photosynthesis and light for phytoplankton. *Limnol. Oceanogr.* **1976**, *21*, 540–547. [[CrossRef](#)]
34. Roleda, M.Y.; Hanelt, D.; Wiencke, C. Exposure to ultraviolet radiation delays photosynthetic recovery in Arctic kelp zoospores. *Photosynth. Res.* **2006**, *88*, 311–322. [[CrossRef](#)] [[PubMed](#)]
35. Klughammer, C.; Schreiber, U. Complementary PS II quantum yields calculated from simple fluorescence parameters measured by PAM fluorometry and the saturation pulse method. *PAM Appl. Notes* **2008**, *1*, 27–35.
36. Ishikawa, Y.; Saga, N. *The Diseases of Economically Valuable Seaweeds and Pathology in Japan*; Miyachi, S., Karube, I., Ishida, Y., Eds.; Fuji Technology Press Ltd.: Tokyo, Japan, 1989; pp. 215–218.
37. Gachon, C.M.M.; Sime-Ngando, T.; Strittmatter, M.; Chambouvet, A.; Kim, G.H. Algal diseases: Spotlight on a black box. *Trends. Plant. Sci.* **2010**, *15*, 633–640. [[CrossRef](#)] [[PubMed](#)]

38. Blake, R.E.; Duffy, J.E. Influence of environmental stressors and grazer immigration on ecosystem properties of an experimental Eelgrass community. *J. Exp. Mar. Biol. Ecol.* **2016**, *480*, 45–53. [[CrossRef](#)]
39. Msuya, F.E.; Matoju, I.; Buriyo, A.; Rusekwa, S.; Shaxson, L.; Le Masson, V.; Nagabhatla, N.; Cottier, E.; De Lombaerde, P. *Coping with Climate Change to Safeguard the Seaweed Industry in Eastern Africa: Spotlight on Tanzania*; United Nations University Institute on Comparative Regional, Integration Studies Policy Brief: Hamilton, ON, Canada, 2022; ISBN 978-9912-40-076-4.
40. Behera, D.P.; Ingle, K.N.; Mathew, D.E.; Dhimmar, A.; Sahastrabudhe, H.; Sahu, S.K.; Krishnan, M.G.; Shinde, P.B.; Ganesan, M.; Mantri, V.A. Epiphytism, diseases and grazing in seaweed aquaculture: A comprehensive review. *Rev. Aquac.* **2022**, *14*, 1345–1370. [[CrossRef](#)]
41. Apt, K.E. Galls and tumor-like growths on marine macroalgae. *Dis. Aquat. Organ.* **1988**, *4*, 211–217. [[CrossRef](#)]
42. McKeown, D.A.; Stevens, K.; Peters, A.F.; Bond, P.; Harper, G.M.; Brownlee, C.; Brown, M.T.; Schroeder, D.C. Phaeoviruses discovered in kelp (*Laminariales*). *ISME J.* **2017**, *11*, 2869–2873. [[CrossRef](#)]
43. Kim, Y.T.; Kim, R.-w.; Shim, E.; Park, H.; Klochkova, T.A.; Kim, G.H. Control of oomycete pathogens during Pyropia farming and processing using calcium propionate. *Algae* **2023**, *38*, 71–80. [[CrossRef](#)]
44. Ding, H.; Ma, J. Simultaneous infection by red rot and chytrid diseases in *Porphyra yezoensis* Ueda. *J. Appl. Phyc.* **2005**, *17*, 51–56. [[CrossRef](#)]
45. Badis, Y.; Klochkova, T.A.; Brakel, J.; Arce, P.; Ostrowski, M.; Tringe, S.G.; Kim, G.H.; Gachon, C.M.M. Hidden diversity in the oomycete genus *Olpidiopsis* is a potential hazard to red algal cultivation and conservation worldwide. *Eur. J. Phycol.* **2020**, *55*, 162–171. [[CrossRef](#)]
46. Porter, D.; Farnham, W.F. *Mycaureola dilseae*, a marine basidiomycete parasite of the red alga, *Dilsea carnosa*. *Trans. Br. Mycol.* **1986**, *87*, 575–582. [[CrossRef](#)]
47. Ma, Y.; Zhang, Z.; Fan, C.; Cao, S. Study on the pathogenic bacteria of spot decay disease of *Undaria pinnatifida* in Dailan. *J. Fis. Sci. China* **1997**, *4*, 62–65.
48. Guiry, M.D. The occurrence of the red algal parasite *Halosaccicolax lundii* Edelstein in Britain. *Brit. Phycol. J.* **1974**, *9*, 31–35. [[CrossRef](#)]
49. Hurtado, A.; Critchley, A.; Trespoey, A.; Lhonneur, G.B. Occurrence of *Polysiphonia* epiphytes in *Kappaphycus* farms at Calaguas Is., Camarines Norte, Philippines. *J. Appl. Phycol.* **2006**, *18*, 301–306. [[CrossRef](#)]
50. Zozaya-Valdés, E.; Roth-Schulze, A.J.; Egan, S.; Thomas, T. Microbial community function in the bleaching disease of the marine macroalgae *Delisea pulchra*. *Environ. Microbiol.* **2017**, *19*, 3012–3024. [[CrossRef](#)] [[PubMed](#)]
51. Sakaguchi, K.-I.; Park, C.S.; Kakinuma, M.; Amano, H. Effects of varying temperature, salinity and acidity in the treatment of *Porphyra* infected by red rot disease. *Aquac. Sci.* **2001**, *49*, 77–83.
52. Kambey, C.S.B.; Campbell, I.; Cottier-Cook, E.J. Seaweed aquaculture: A preliminary assessment of biosecurity measures for controlling the ice-ice syndrome and pest outbreaks of a *Kappaphycus* farm. *J. Appl. Phycol.* **2021**, *33*, 3179–3197. [[CrossRef](#)]
53. Kinnby, A.; Gunilla, T.B.; Henrik, P. Climate Change Increases Susceptibility to Grazers in a Foundation Seaweed. *Front. Mar. Sci.* **2021**, *8*, 688406. [[CrossRef](#)]
54. Kramer, D.M.; Johnson, G.; Kiirats, O.; Edwards, G.E. New fluorescence parameters for the determination of QA redox state and excitation energy fluxes. *Photosynth. Res.* **2004**, *79*, 209–218. [[CrossRef](#)]

Disclaimer/Publisher’s Note: The statements, opinions and data contained in all publications are solely those of the individual author(s) and contributor(s) and not of MDPI and/or the editor(s). MDPI and/or the editor(s) disclaim responsibility for any injury to people or property resulting from any ideas, methods, instructions or products referred to in the content.